Closed-Form Analysis of Reflection Losses in Microstrip Reflectarray Antennas

Filippo Costa, *Member, IEEE*, and Agostino Monorchio, *Fellow, IEEE*

***Abstract*—Microstrip reflectarray antennas consist of a grounded quasi-periodic array of printed elements able to compensate the phase displacement of a non-coherent electromagnetic excitation generated by a feeder. The design of reflectarray antennas is usually accomplished by tracing the reflection phase diagram of the periodic version of the printed surface, which is analogous to a high-impedance surface (HIS). Reflection losses of this periodic structure are here analyzed through a simple equivalent transmission line model. The analytical expressions of the surface impedance offered by a HIS (real and imaginary part) as a function of the imaginary part of the dielectric permittivity of the substrate are derived through well justified approximations. Some useful practical examples are then presented both for verifying the accuracy of the derived closed-form expressions and for studying the effect of the geometrical and electrical parameters of the periodic surface on the reflection losses. The dependence of the input impedance on the capacitance associated with the printed pattern is highlighted, demonstrating that highly capacitive elements (tightly coupled subwavelength elements) are preferable for minimizing reflection losses.**

***Index Terms*—Frequency Selective Surfaces (FSS), high-impedance surfaces, losses, microstrip reflectarray antennas.**

I. Introduction

MICROSTRIP reflectarray antennas consist of a 2D quasi-periodic pattern printed over a grounded substrate. The reflecting structure transforms the field radiated by the feeder into a phase-coherent [1], [2] or shaped beam [3], [4] towards a desired direction. The focusing or shaping effect can be achieved by slightly modifying the shape or size of the printed elements in order to locally vary the phase of the reflected field. A basic step in the design of reflectarray antennas is the calculation of the reflection phase diagram, reporting the phase of the reflection coefficient versus a relevant geometrical dimension of the element. Due to the quasi-periodicity of the structure, the phase diagram can be calculated under the infinite periodic array assumption. The periodic version of a printed reflectarray antenna is analogous to a high-impedance surface [5]. HIS structures are usually employed in the design of several microwave devices such as ultra-thin electromagnetic absorbers [6], low-profile antennas [7], Fabry-Perot/Leaky wave antennas [8], for simultaneous switching noise (SSN) suppression in PCB circuits [9] and additional applications [10].

Reflectarray antennas, differently from HIS structures, are usually designed with half wavelength spaced elements but we remark that Frequency Selective Surfaces (FSSs) with densely packed elements or $\lambda/2$ spaced elements are equivalent from a circuital point of view. The use of compact patch arrays leads to bandwidth maximization [11]–[13].

In the design of a reflectarray it is desirable that the reflection phase diagram as a function of a geometrical parameter presents a limited slope near the resonance so that a small change in the element size (due to fabrication inaccuracies) weakly influences the reflection phase response [14]. An additional requirement of reflectarray antennas is a wide operating bandwidth, i.e., a limited variation of the phase reflection coefficient as a function of the frequency [13]. The latter property can be verified by tracing the phase diagram versus frequency for every chosen dimension of the element.

Printed antennas like reflectarrays are realized by employing commercial substrates characterized by a loss component. Reflection losses of reflectarray antennas are mainly due to the dielectric loss tangent and the conductivity of the metal since surface wave losses are indeed limited [1]. A simple approach for analyzing the effect of metal and dielectric losses of printed reflectarray is presented in [15] where some of the most common elements are analyzed without anyway drawing general guidelines for achieving low reflection losses. In [16] and [17] reflection losses arising from the use of various substrates are discussed and quantified with a methodical analysis.

In this paper, the effect of dielectric and ohmic losses is analytically investigated by deriving closed-form expressions. The analytical derivations are based on a simple transmission line model approximation of the periodic structure. The derived expressions allow one to clarify the mechanisms causing the reflection losses and they are rigorously verified through comparison with full-wave results. It is shown that the real part of the input impedance of the structure, which determines the amplitude of the reflection coefficient, contains two separate terms: one due to the loss of the substrate itself whereas the other is due to the presence of the periodic array on the top of a lossy substrate. Once the closed-form expressions are derived, it is also possible to deduce the influence of the substrate thickness and the dielectric loss tangent on the reflection amplitude reduction. More importantly, the effect of the unit cell shape is discussed demonstrating that the use of tightly coupled subwavelength elements is beneficial for minimizing reflection losses.

Manuscript received April 09, 2011; revised October 19, 2011; accepted May 11, 2012. Date of publication July 10, 2012; date of current version October 02, 2012.

The authors are with the Dipartimento di Ingegneria dell'Informazione, University of Pisa, Via G. Caruso 16, 56122 Pisa, Italy and also with RaSS National Lab, CNIT, Galleria Gerace 18, 56124, Pisa, Italy (e-mail: filippo.costa@iet.unipi.it; a.monorchio@ieee.org).

Color versions of one or more of the figures in this paper are available online at http://ieeexplore.ieee.org.

Digital Object Identifier 10.1109/TAP.2012.2207318

The paper is organized as follows: in the next Section, the impedance of a periodic metallic array printed on a lossy substrate is derived. Section III is dedicated to the calculation of the input impedance of a grounded lossy substrate. In Section IV the real and the imaginary parts of the input impedance of the entire resonant structure is calculated by merging the results achieved in the two previous sections. Section V presents some examples aimed to verify the validity of the derived closed-form expressions and to show the absorption mechanisms of reflectarray antennas. Finally, in Section VI, the effect of oblique incidence is assessed.

II. Impedance of a Periodic Array Printed on a Lossy Substrate

The planar structure employed to design reflectarray antennas consists of a quasi-periodic array of patches or more exotic elements over a thin grounded dielectric slab. Due to the quasi-periodicity, losses of the structure can be analyzed under the infinite periodic array assumption. The layout of the investigated structure and its equivalent circuit are reported in Fig. 1. The periodic array on the top of the grounded substrate is basically a capacitive Frequency Selective Surface (FSS) behaving as a capacitor in the low frequency region while its impedance becomes inductive after the resonance. The impedance of a FSS made of Perfect Electric Conductor (PEC) can be represented through a series LC circuit or, more simply, by a single capacitor if the inductive component is low (e. g. square patch element). The accuracy of the LC model extends from the DC to the onset of grating lobes, that is, when the repetition period of the unit cell approaches one wavelength [18]. If the patch array is represented by a capacitor only, the accuracy is guaranteed up to a spacing of $\lambda/2$ [18]. When an FSS is printed on a lossy dielectric substrate, the value of the unloaded capacitor has to be multiplied by the effective dielectric permittivity due the surrounding dielectrics [18]. If the condition of sufficiently thick substrate is verified (thicker than $0.3D$, being D the FSS periodicity [18], [19]), the effective permittivity simply corresponds to the average of the relative permittivity of the substrate ($\varepsilon_r = \varepsilon_r' + j\varepsilon_r''$) and the relative permittivity of free space [20]:

$$\varepsilon_{eff} = \frac{(\varepsilon_r + 1)}{2} = \frac{(\varepsilon_r' + 1)}{2} + j\frac{\varepsilon_r''}{2} \tag{1}$$

According to (1), the lumped impedance Z_{FSS} of the PEC FSS printed on a lossy substrate is therefore composed by a real and an imaginary term:

$$Z_{FSS} = \frac{1 - \omega^2 LC_0\varepsilon_{eff}}{j\omega C_0\varepsilon_{eff}} = R_D + jX \tag{2}$$

Under small losses assumption, i.e.,$\varepsilon_r' \gg \varepsilon_r''$, and assuming that the resonance frequency of the HIS is smaller or much smaller than the FSS resonance frequency $\omega_{FSS} = 2/[LC_0(\varepsilon_r' + 1)]$, the resistor representing the loss component of the FSS caused by the surrounding lossy dielectric, approximately reads:

$$R_D \simeq \frac{-2\varepsilon_r''}{\omega C_0 \left(\varepsilon_r' + 1\right)^2} \tag{3}$$

where C_0 represents the capacitance of the periodic structure in freestanding configuration (unloaded capacitance). Under the same small losses assumption, the imaginary part of the FSS impedance X is almost equal to the reactance of the PEC FSS impedance:

$$X \simeq -\frac{1 - \omega^2 LC_0 \frac{(\varepsilon_r' + 1)}{2}}{\omega C_0 \frac{(\varepsilon_r' + 1)}{2}} \tag{4}$$

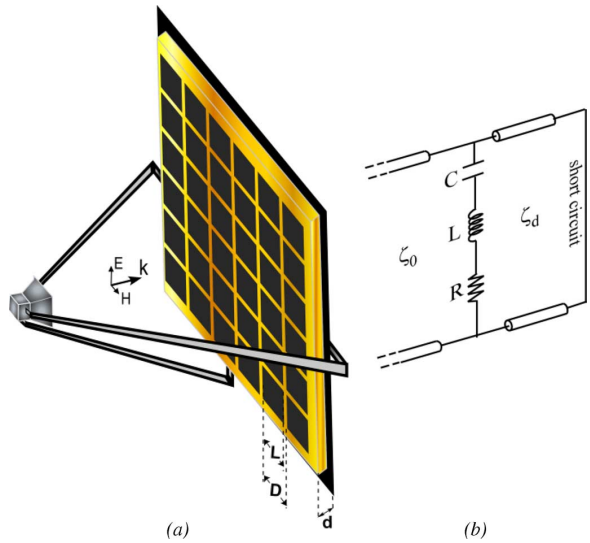

Fig. 1. 3D sketch of the analyzed structure (a) and its equivalent circuit (b). C is the effective capacitance of the FSS printed on the substrate, that is $C_0(\varepsilon_r' + 1)/2$; L is the FSS inductance and R is the resistor which takes into account dielectric and ohmic losses, i.e. $R = R_D + R_O$.

If a real authentic metallic FSS is considered, ohmic losses should be included within the FSS impedance through an additional series resistance R_o:

$$Z_{FSS} = R_o + R_D + jX = R + jX \tag{5}$$

Here, the resistor accounting for ohmic losses is neglected since, within the microwave range, its value is almost two order of magnitude lower than the resistor due to dielectric losses. The two resistors account for two different physical phenomena. Let us consider a plane wave striking a FSS (e.g. a patch array); the impinging wave excites current on the periodic surface creating a parallel plate capacitor between the edges of adjacent patches where the electric field is rather strong. While ohmic losses come from the currents flowing on the imperfect conductor, the resistor R_D accounts for the loss component of the capacitor formed between the adjacent elements, being electric field lines concentrated in a lossy medium. Such loss component is readily represented by a resistor in parallel with the lossless capacitor [19], but for our purpose, it is more convenient to transform the parallel circuit into a series connection of a capacitor and a resistor as in (3) and (4). A schematic representation of the lumped components associated with the described physical phenomena is reported in Fig. 2.

The unloaded capacitance and the inductance of the FSS are computed by matching the normal incidence full-wave response of the elements in freestanding configuration [18], [19]. Alternatively, if a square patch element is employed, the capacitance

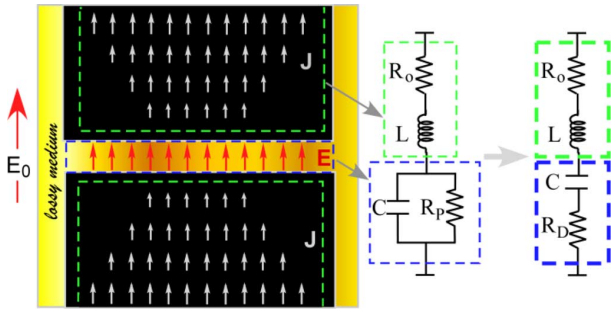

Fig. 2. Qualitative representation of the currents and the electric field excited within the unit cell of a patch FSS and the correspondent lumped elements.

can be approximated by the following closed-form expression [20]:

$$C_0^{patch} = \frac{2D\varepsilon_0}{\pi} \ln\left(\frac{1}{\sin\left(\frac{\pi w}{2D}\right)}\right) \tag{6}$$

being D the periodicity of the periodic array, w (or $D-L$) the gap between the patches and ε_0 the dielectric permittivity of free space. However, as already mentioned, the accuracy of the model under this approximation is guaranteed up to a spacing of $\lambda/2$ [18]. For this reason, we will employ the LC series model of the FSS.

If the periodic surface is printed over a thin dielectric substrate, the influence of higher-order (evanescent) Floquet modes reflected by the ground plane cannot be neglected. The influence of the evanescent modes in the equivalent model can be taken into account by the following substitution [22]:

$$C_0^{thin} = C_0 - \frac{2D\varepsilon_0}{\pi} \ln\left(1 - e^{-\frac{4\pi d}{D}}\right) \tag{7}$$

where d represents the thickness of the dielectric substrate. As the dielectric thickness diminishes, we have an increase of the capacitance due to the capacitor created between the FSS and the ground plane.

III. Input Impedance of a Grounded Lossy Substrate

The input impedance of a lossy grounded dielectric slab Z_d at normal incidence, reads:

$$Z_d = j\frac{\zeta_0}{\sqrt{\varepsilon_r' + j\varepsilon_r''}} \tan\left(k_0\sqrt{\varepsilon_r' + j\varepsilon_r''}d\right) \tag{8}$$

where ζ_0 is the characteristic impedance of free space; k_0 is the free space propagation constant and d is the thickness of the dielectric substrate. In order to derive the real and the imaginary part of the input impedance, Z_d, it is necessary to manipulate the terms containing complex numbers. By assuming $\varepsilon_r' \gg \varepsilon_r''$, the real and the imaginary parts (named A and B respectively, for convenience) of the input impedance can be expressed as follows (see Appendix I):

$$\mathrm{Re}\{Z_d\} = A \cong \frac{\zeta_0}{\sqrt{\varepsilon_r'}}\left[\frac{\varepsilon_r''}{2\varepsilon_r'}\tan\left(k_0 d\sqrt{\varepsilon_r'}\right) - \left(k_0 d\frac{\varepsilon_r''}{2\sqrt{\varepsilon_r'}}\right) \times \left(1 + \tan^2\left(k_0 d\sqrt{\varepsilon_r'}\right)\right)\right] \tag{9}$$

$$\mathrm{Im}\{Z_d\} = B \cong \frac{\zeta_0}{\sqrt{\varepsilon_r'}}\left[\tan\left(k_0 d\sqrt{\varepsilon_r'}\right)\right] \tag{10}$$

The term A depends on both the real and imaginary parts of the dielectric permittivity, whereas B is weakly influenced by the loss component of the substrate dielectric permittivity. The dielectric losses associated with the real part of the input impedance are due to the interaction of electric fields crossing the metallic array with the lossy dielectric. In Section V it will be demonstrated that, in most of the practical cases, this contribution is negligible with respect to the FSS resistance.

IV. Input Impedance of a HIS Structure as a Function of the Substrate Loss

In the previous sections, the impedance of the periodic printed surface and the input impedance of the lossy grounded substrate have been expressed as two complex numbers characterized by a real and an imaginary part. The input impedance of the HIS (or reflectarray) structure Z_R is equal to the parallel connection between the two complex impedances $Z_{FSS}(R+jX)$ and $Z_d(A+jB)$. After some simple algebra, the real and imaginary terms of Z_R can be expressed as follows:

$$\mathrm{Re}\{Z_R\} = \frac{(AR - BX)(A+R) + (BR - XA)(B+X)}{(A+R)^2 + (B+X)^2} \tag{11}$$

$$\mathrm{Im}\{Z_R\} = \frac{X(A^2 + BX) + B(R^2 + BX)}{(A+R)^2 + (B+X)^2} \tag{12}$$

If $A = 0$ the formulation resembles the case of thin resistive HIS absorbers [6] in which only ohmic losses are retained. For an ideal lossless structure, the resonance condition is achieved as the imaginary part of the input impedance Z_R goes to infinity. An actual HIS structure employing a low-loss substrate is instead characterized by a very high real part and by a smooth transition through zero of the imaginary part [6]. The denominator of (12) goes to infinity in the vicinity of the resonance, but the condition $X = -B$ in the presence of small losses, does not determine a pole in (12) but a zero, being $B \gg A$ and $B \gg R$ (see Appendix II).

The magnitude of the reflection coefficient of the periodic structure at the resonance, assuming the imaginary part of Z_R equal to zero, reads approximately:

$$|\Gamma| \approx \frac{\mathrm{Re}\{Z_R\} - \zeta_0}{\mathrm{Re}\{Z_R\} + \zeta_0} \tag{13}$$

The amount of losses of the resonant cavity is basically determined by the value of the real part of the input impedance. A very large real part leads to a limited amount of reflection losses. As the real part of the input impedance decreases down to the free space impedance, the HIS structure performs an increasing absorption of the incoming signal instead of the desired total reflection. By assuming $X = -B$, the real part of Z_R derived in (11) simplifies as follows:

$$\mathrm{Re}\{Z_R^{res}\} = \frac{(AR + B^2)}{(A+R)} \cong \frac{B^2}{(A+R)} \tag{14}$$

since $B \gg A, R$. By replacing the relations (3), (9), (10) in (14), the real part of the input impedance at the resonance can

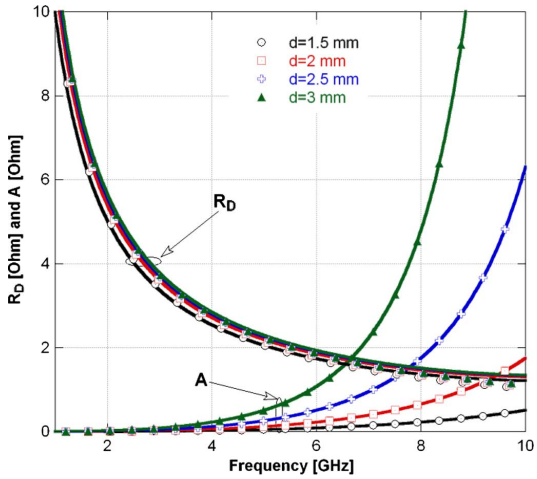

Fig. 3. Real part of the FSS impedance (R_D) and real part of the grounded substrate input impedance (A) for various substrate thicknesses. Solid lines: MoM simulations; symbols: TL model.

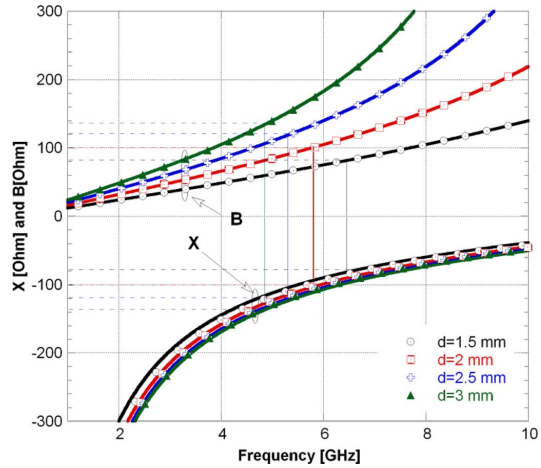

Fig. 4. Imaginary part of the FSS impedance (X) and imaginary part of the grounded substrate input impedance (B) for various substrate thicknesses. The resonance condition $B = -X$ is highlighted. Solid lines: MoM simulations; symbols: TL model.

be explicitly written (see relation (15) at the bottom of the page). Since the resistance of the FSS, R_D, due to the presence of the lossy dielectric substrate, is always larger than the real part of the input impedance of the grounded dielectric slab, A, up to the first resonance of the HIS structure (see the analytical demonstration in Appendix III), the relation (15) can be further simplified up to the first resonance ω_0 as:

$$\mathrm{Re}\left\{Z_R^{res}\right\} \approx \frac{\zeta_0^2 \left[\tan^2\left(k_0 d\sqrt{\varepsilon_r'}\right)\right] \omega C_0 \left(\varepsilon_r'+1\right)^2}{-2\varepsilon_r''\varepsilon_r'} \quad \text{if } \omega < \omega_0 \tag{16}$$

The expression of the real part of Z_R in (16) is a function of the capacitance C_0 of the FSS, the substrate thickness, the real and the imaginary parts of the dielectric permittivity. The increase of dielectric losses, ε'', leads to a reduction of the real part of the input impedance towards the free space impedance with a consequent reflection loss increase. The other parameters are analyzed in detail through the following examples.

V. Numerical Examples and Model Validation

A set of numerical examples is proposed both to clarify the reflection loss behavior as a function of the main parameters of the reflectarray and to verify the above derived analytical relations. The results achieved by analytical expressions are verified by a full-wave analysis based on the Method of Moments [23].

1) Square Patch Array on an FR4 Slab With Various Thicknesses: Let us consider a simple square patch FSS printed on a commercial FR4 substrate ($\varepsilon_r = 4.5 - \mathrm{j}0.088$). The period D of the FSS is chosen equal to 10 mm and the dimension of the metallic patch L is equal to 8.75 mm ($L = 7/8D$). The real part of the FSS impedance, R_D, and the real part of the grounded substrate input impedance, A, are compared in Fig. 3 for various substrate thicknesses. It is apparent that R_D value is much larger than A value before the resonance. This verifies the approximation used for obtaining the relation (16). The reactance of the above mentioned impedances is plotted in Fig. 4.

The resonance condition of the HIS cavity is verified as the imaginary parts of the plotted impedances assume the same value and opposite sign. Fig. 5 reports the real and the imaginary parts of Z_R together with its transmission line model approximations (relations (11) and (12)) for various substrate thicknesses.

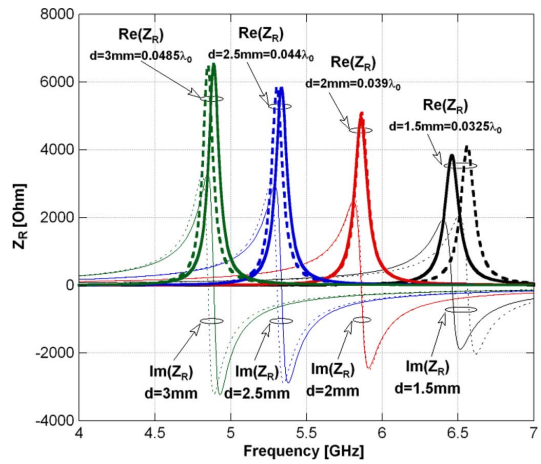

Fig. 5. Real and imaginary part of the HIS input impedance Z_R for various substrate thicknesses. Substrate dielectric permittivity: (4.5-j0.088). Patch side $L : 14/16D$, with $D = 10$ mm. Solid lines: MoM simulations; dashed lines: TL model (relations (11) and (12)).

$$\mathrm{Re}\left\{Z_R^{res}\right\} = \frac{\frac{\zeta_0^2}{\varepsilon_r'}\left[\tan^2\left(k_0 d\sqrt{\varepsilon_r'}\right)\right]}{\frac{-2\varepsilon_r''}{\omega C_0(\varepsilon_r'+1)^2} - \frac{\zeta_0}{\sqrt{\varepsilon_r'}}\left[\left(k_0 d\frac{\varepsilon_r''}{2\sqrt{\varepsilon_r'}}\right)\left(1+\tan^2\left(k_0 d\sqrt{\varepsilon_r'}\right)\right) - \frac{\varepsilon_r''}{2\varepsilon_r'}\tan\left(k_0 d\sqrt{\varepsilon_r'}\right)\right]} \tag{15}$$

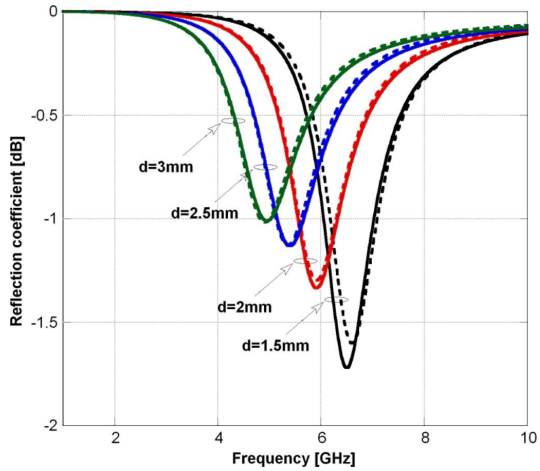

Fig. 6. Reflection coefficient of the HIS for various substrate thicknesses. Solid lines: MoM simulations; dashed lines: TL model.

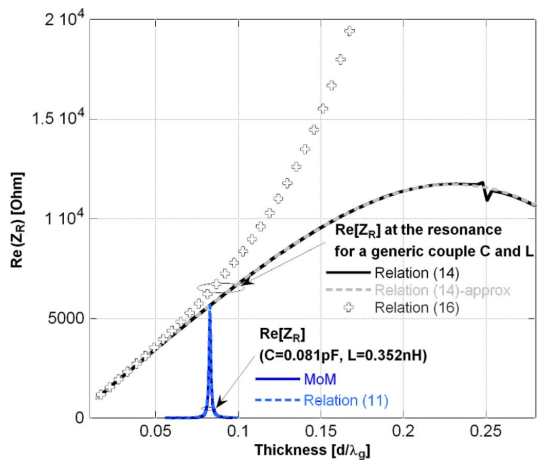

Fig. 7. Real part of the input impedance of the HIS at a fixed resonance frequency for a 2 mm thick FR4 substrate. The capacitance included in the FSS resistor is computed according to (17). The plot reports also the real part of the input impedance for one of the specific cases analyzed above (i.e. square patch FSS with $L = 14/16$, $D = 10$ mm).

As the substrate thickness is increased, the resonance frequency is shifted towards lower frequencies proportionally to the square root of the substrate inductance ($\omega_0 \approx 1/\sqrt{L_s C}$ where L_s is the substrate inductance and C is the FSS capacitance).

From (16), it is evident that the increase of the substrate thickness leads to a rise of the real part of the HIS input impedance proportional to B^2 at the resonance. The electrical increase of the thickness is lower than the physical one because of the shift of the resonance towards higher wavelengths. In Fig. 6 the reflection coefficient of the HIS is shown for different substrate thicknesses. The use of a thick substrate leads to lower losses than a thin substrate because of the higher real part of the input impedance. Let us now analyze the behavior of the real part of the input impedance at the resonance as a function of the frequency or, equivalently, of the electrical substrate thickness. Fig. 7 reports the real part of the input impedance of the HIS computed at the resonance independently of the capacitive load of the FSS. The quantity is drawn on the basis of three different approximations: the curves defined by the first and the second form of (14) and the curve computed according to (16). The capacitance included in the expression of the FSS resistor is computed by using relation (17) in order to keep the resonance at a fixed frequency. The first two curves overlap since the approximation $B \gg A, R$, adopted in (14), holds for every substrate thickness. The curve calculated through relation (16) follows the aforementioned ones up to the first resonance since the approximation $R > A$ is valid, as remarked in the Appendix III, only before the first resonance of the structure and for substrate thickness lower than $\lambda_g/8$. As these conditions are not fulfilled, the approximation $R > A$ (see Fig. 3) is not valid and the real part of the HIS input impedance Z_R depends also on the real part of the grounded substrate impedance, A. In the latter case the increase of the substrate thickness (or equivalently the increase of the frequency) does not determine a monotonic rise of the real part of the input impedance. The electrical thickness leading to the maximum of Z_R is due to the interaction between the expressions at the denominator of (15) but it is close to $\lambda_g/4$.

2) Square Patch Array With Variable Gap and Fixed Periodicity on a 2 mm FR4 Slab: The enhancement of the capacitive coupling between the printed elements leads to a shift towards lower frequencies of the resonance frequency (the shift is proportional to the square root of the FSS capacitance C) which means lower electrical thickness of the substrate. Since thickness reduction and capacitance increase are conflicting trends, it is useful to remove the dependence on the capacitance from (16). Considering for simplicity an FSS made of patch array represented by a capacitance only [19], the following relation holds at the resonance:

$$\frac{1}{\omega C_0 \left(\frac{\varepsilon_r'+1}{2}\right)} \approx \frac{\zeta_0}{\sqrt{\varepsilon_r'}} \left[\tan\left(k_0 d \sqrt{\varepsilon_r'}\right)\right] \tag{17}$$

By substituting the relation (17) in (16), we get:

$$\mathrm{Re}\left\{Z_R^{res}\right\} \approx -\frac{\left(\varepsilon_r'+1\right)\zeta_0}{\varepsilon_r''\sqrt{\varepsilon_r'}} \left[\tan\left(k_0 d \sqrt{\varepsilon_r'}\right)\right] \quad \text{if} \quad \omega < \omega_0 \tag{18}$$

At this stage the input impedance of the structure at the resonance is expressed only by substrate parameters. It can be observed that the effect of the substrate thickness reduction dominates on the increase of the capacitance value and the real part of the input impedance at the resonance is reduced. This leads to an increase of the reflection loss as reflection coefficient amplitude curves of Fig. 8 confirm.

3) Square Patch Array FSS Element With Variable Gap and Variable Periodicity Printed on a 2 mm FR4 Substrate: If the shift towards lower frequencies due to capacitive coupling enhancement is compensated by a reduction of the FSS periodicity, it is possible to observe the effect of the elements spacing at a fixed frequency. While the patch gap is made narrower, the FSS periodicity is reduced in order to maintain the FSS reactance fixed, that is, the FSS inductance decreases while the capacitance increases [13]. In Fig. 9 and Fig. 10 the phase and the magnitude of the reflection coefficient are reported at a fixed frequency for various spacings of the patch array.

The enhancement of the capacitance at a fixed frequency with fixed substrate parameters, leads to a strong reduction of the

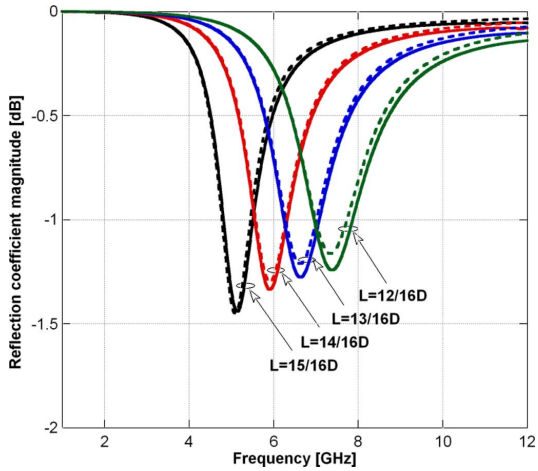

Fig. 8. Reflection coefficient magnitude of the HIS for various patch gap sizes. Substrate thickness: 2 mm. Dielectric permittivity: (4.5-j0.088). Solid lines: MoM simulations; dashed lines: TL model.

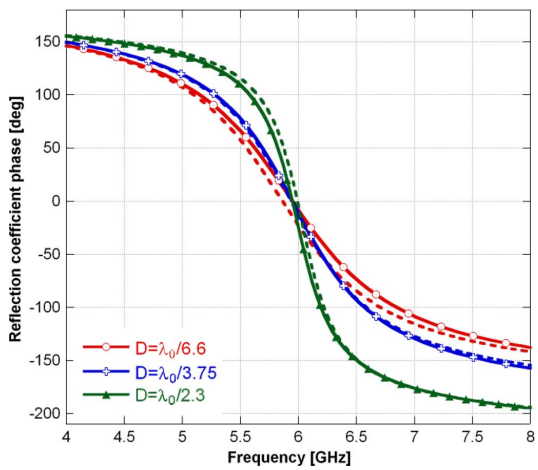

Fig. 9. Reflection coefficient phase of the HIS for various spacing of the printed elements. The element size is chosen so that the resonance frequency is constant. The substrate thickness is 2 mm and its dielectric permittivity is: 4.5-j0.088. Solid lines: MoM simulations; dashed lines: TL model.

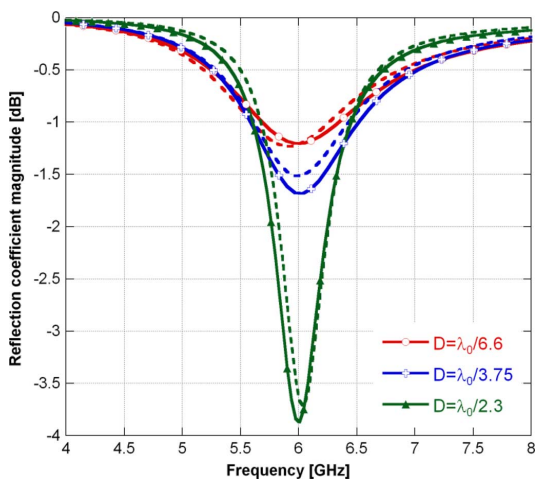

Fig. 10. Reflection coefficient magnitude of the HIS for various spacing of the printed elements. The element size is chosen so that the resonance frequency is constant. The substrate thickness is 2 mm and its dielectric permittivity is (4.5-j0.088). Solid lines: MoM simulations; dashed lines: TL model.

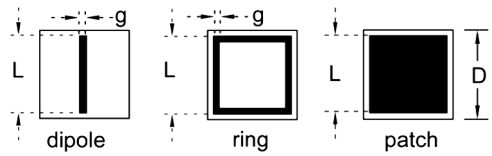

Fig. 11. Investigated unit cell elements.

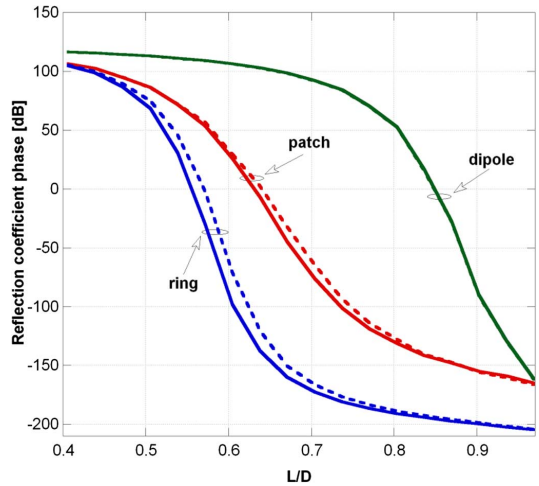

Fig. 12. Phase reflection coefficient of three FSS elements printed on top of a grounded 2.5 mm FR4 substrate at 8 GHz as a function of the size L. Cell periodicity D: 10 mm. Solid lines: MoM simulations; dashed lines: TL model.

reflection losses. Similar results have been recently achieved in [24], [25] with a parametric analysis.

As is apparent, the usual practice of designing reflectarrays with $\lambda/2$ spaced elements is not the best configuration for bandwidth maximization or loss minimization. The choice of closely spaced patches, as earlier observed in [12], [26] and formally demonstrated in [13], leads to a one layer reflectarray with the widest possible bandwidth for a fixed substrate thickness. Similar subwavelengh printed FSS configurations have also been employed in the design of wideband antenna arrays [27].

4) Fixed Periodicity FSS Element With Variable Size Printed on a 2.5 mm FR4 Substrate: In order to derive the desired reflection phase coefficient for a given position of the array, the reflection phase characteristic of the structure as a function of the element size is usually analyzed at a fixed frequency. It is desirable that the slope of such phase diagram is as slow as possible so that potential fabrication inaccuracies will not produce remarkable variation of the performance. The focusing effect of the antenna is achieved by progressively modifying the size of the printed elements with the aim of locally varying the reflection phase coefficient of the surface. When the phase excursion guaranteed by a single layer reflectarray is not sufficient, a double layer structure is employed [3], [4].

Three standard FSS elements are analyzed in order to derive a general criterion for the design of a low-loss reflectarray antenna. Fig. 11 shows the elements under investigation.

In Fig. 12 the phase reflection coefficient of the three periodic arrays on the top of a 2.5 mm grounded FR4 substrate is shown at 8 GHz as a function of the physical dimension L. The

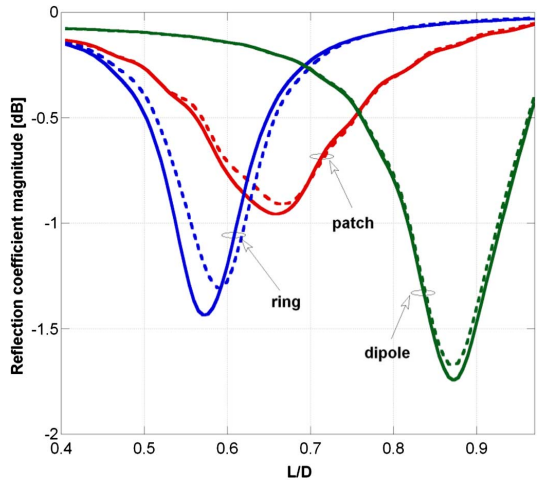

Fig. 13. Reflection coefficient magnitude of three FSS elements on the top of a grounded 2.5 mm FR4 substrate at 8 GHz as a function of the size L. Cell periodicity D: 10 mm. Solid lines: MoM simulations; dashed lines: TL model.

TABLE I
VALUES OF THE CAPACITANCE AND INDUCTANCES OF THE ANALYZED ELEMENTS AT THE RESONANCE (I.E. 8 GHz). THE RATIO L/D FOR EACH ELEMENT AT THE RESONANCE IS ALSO REPORTED

	C [pF]	L [nH]	L/D
Patch	0.027	1.42	0.62
Ring	0.0163	4.55	0.55
Cross	0.0139	6.83	0.85

unit cell periodicity is fixed at 10 mm. Fig. 13 reports the reflection losses of the printed arrays as a function of the physical dimension L. The square patch element is characterized by the smallest amount of losses since the capacitance of the element at the resonance is the highest. Indeed, in accordance to (16), the maximization of the capacitance at the resonance, keeping the other parameters fixed, leads to a smallest amount of loss. It has anyway to be observed that the patch array is characterized by a more limited phase excursion with respect to ring or dipole elements. The capacitances and the inductances of the analyzed elements at the resonance are summarized in Table I. The values of the lumped components are computed by matching the normal incidence full-wave response of the elements in freestanding configuration [18]. As it is observable, the square patch capacitance leading to the resonance at 8 GHz (i.e. $C = 0.027$ pF at $L/D = 0.62$) is larger than the capacitances of the other two elements (ring: $C = 0.0163$ pF at $L/D = 0.55$, dipole: $C = 0.0139$ pF at $L/D = 0.85$).

The capacitance of an FSS element increases as the coupling area is maximized and the distance between the adjacent metal conductors is reduced. On the contrary, the inductance of a printed structure, according to the expression reported in [28], decreases as the element is made larger or longer keeping the substrate parameters fixed.

VI. OBLIQUE INCIDENCE

As the incident angle is off normal with respect to the surface, the input impedance of the structure varies since both the grounded substrate input impedance Z_d and the FSS impedance Z_{FSS} are angle dependent [19]. The analysis performed in Section IV is still valid after the substitution of the expressions valid at oblique incidence.

The expression of the grounded substrate input impedance at oblique incidence reads:

$$Z_d = jZ_m^{TE,TM}\tan\left(k_0 d\sqrt{\varepsilon_r' + j\varepsilon_r'' - \sin^2(\vartheta)}\right) \tag{19}$$

where $Z_m^{TE} = (\omega\mu_r\mu_0)/\beta$; $Z_m^{TM} = \beta/(\omega\varepsilon_r\varepsilon_0)$ are the characteristic impedances of the slab for TE and TM polarization, $\beta = k_0\sqrt{\varepsilon_r - \sin^2(\vartheta)}$ is the propagation constant along the normal unit of the slab and θ is the incidence angle of the incoming wave with respect to the normal. In order to compute the real and the imaginary part of the of the grounded substrate input impedance, the same approximations described in Section III and in the appendix are used. The expressions for TE and TM polarization are the following:

$$\begin{aligned} A^{TE} \cong & \frac{\zeta_0}{\sqrt{\varepsilon_r' - \sin^2(\vartheta)}} \\ & \times\left\{\left[\frac{\varepsilon_r''}{2\left(\varepsilon_r' - \sin^2(\vartheta)\right)}\right]\tan\left(k_0 d\sqrt{\varepsilon_r' - \sin^2(\vartheta)}\right)\right. \\ & -\left(k_0 d\frac{\varepsilon_r''}{2\sqrt{\varepsilon_r' - \sin^2(\vartheta)}}\right) \\ & \left.\times\left(1+\tan^2\left(k_0 d\sqrt{\varepsilon_r' - \sin^2(\vartheta)}\right)\right)\right\} \\ B^{TE} \cong & \frac{\zeta_0}{\sqrt{\varepsilon_r' - \sin^2(\vartheta)}}\left[\tan\left(k_0 d\sqrt{\varepsilon_r' - \sin^2(\vartheta)}\right)\right] \end{aligned} \tag{20}$$

$$\begin{aligned} A^{TM} \cong & \frac{\zeta_0\sqrt{\varepsilon_r' - \sin^2(\vartheta)}}{\varepsilon_r'} \\ & \times\left\{\left[\frac{\varepsilon_r''}{\varepsilon_r'} - \frac{\varepsilon_r''}{2\left(\varepsilon_r' - \sin^2(\vartheta)\right)}\right]\right. \\ & \times\tan\left(k_0 d\sqrt{\varepsilon_r' - \sin^2(\vartheta)}\right) \\ & -\left(k_0 d\frac{\varepsilon_r''}{2\sqrt{\varepsilon_r' - \sin^2(\vartheta)}}\right) \\ & \left.\times\left(1+\tan^2\left(k_0 d\sqrt{\varepsilon_r' - \sin^2(\vartheta)}\right)\right)\right\} \\ B^{TM} \cong & \frac{\zeta_0\sqrt{\varepsilon_r' - \sin^2(\vartheta)}}{\varepsilon_r'}\left[\tan\left(k_0 d\sqrt{\varepsilon_r' - \sin^2(\vartheta)}\right)\right] \end{aligned} \tag{21}$$

It can be observed that the contribution of the real part of the relative dielectric permittivity is somewhat mitigated by the increase of the incident angle. This is the reason why the use of high permittivity substrates calls for an angle stable structure. Similarly, the use of a thin dielectric substrate limits the effect of the incidence angle. In order to highlight the variations of the input impedance as a function of the incident angle, it is useful to simplify the above expressions under the assumption of thin dielectric substrate (which is reasonable in the vicinity of the

HIS resonance). In the latter case, the real and the imaginary parts of the TE and TM impedance read:

$$A^{TE} \approx -\frac{\varepsilon_r''}{2}\zeta_0(k_0 d)^3$$
$$B^{TE} \approx \zeta_0 k_0 d \tag{22}$$
$$A^{TM} \approx -\varepsilon_r''\frac{\zeta_0}{\varepsilon_r'}k_0 d\left(1-\frac{\varepsilon_r'-\sin^2(\vartheta)}{\varepsilon_r'}\right)$$
$$B^{TM} \approx \frac{\zeta_0\left(\varepsilon_r'-\sin^2(\vartheta)\right)}{\varepsilon_r'}k_0 d \tag{23}$$

The TE angular dependence is limited if the dielectric thickness is small compared to the wavelength. The real part of the grounded substrate input impedance for TM polarization increases proportionally to the incident angle. The effect of the incident angle is relevant low dielectric constant substrates since the real part of Z_d becomes comparable to the real part of the FSS impedance. The imaginary part of the Z_d impedance, which appears on the numerator (14), decreases as the incident angles increases.

Let us now analyze the angular dependence of the FSS resistance: it is inversely proportional to the FSS capacitance which is angle dependent only for TE polarization [20]. Its expression is the following:

$$R_D^{TE} \simeq \frac{-2\varepsilon_r''}{\omega C_0\left(\varepsilon_r'+1-\sin^2(\vartheta)\right)^2} \tag{24}$$

The TE FSS resistance increases proportionally to the incidence angle.

By applying the aforementioned arguments to relation (14), we achieve the following guidelines: the real part of the HIS input impedance Z_R decreases for TM polarization while it is almost unchanged for TE incidence. However, when computing the reflection coefficient, it has to be taken into account that the TM free space impedance drops as the incident angle rises ($Z_0^{TM} = Z_0\cos(\vartheta)$), that is, a given value of the input impedance leads to lower losses at TM oblique incidence than at normal incidence. The opposite is valid for TE incidence since $Z_0^{TE} = Z_0/\cos(\vartheta)$.

In conclusion, reflection losses for a TE polarized oblique incidence wave are larger than the normal incidence ones. On the contrary, losses for a TM polarized wave are usually smaller than normal incidence case if a high or moderately high dielectric constant is employed.

As an example, the oblique incidence behavior of a high-impedance surface comprising square patches printed on a 3 mm thick FR4 slab is analyzed. In Fig. 14 the real part of the substrate input impedance A and the FSS resistance for TE and TM polarization computed with MoM approach and with the analytical relations are shown. The incident angle is 60°. Fig. 15 reports the reflection coefficients for TE and TM polarization computed both by the MoM approach and by the transmission line method.

As previously remarked, the reflection losses at oblique incidence increase for TE polarization because of the higher free space impedance and of the higher FSS resistance with respect to the normal incidence. Conversely, in the analyzed case, the reflection losses for TM polarized waves diminish. However, it has to be pointed out that the effect of the oblique incidence can

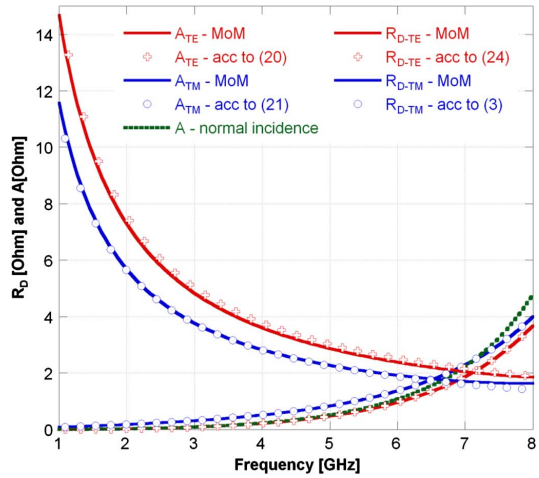

Fig. 14. Real part of the FSS impedance (R_D) and real part of the grounded substrate input impedance (A) for TE and TM polarization. Square patch with $D = 10$ mm. Substrate: thickness 3 mm; dielectric permittivity: 4.5-j0.088. Incident angle: 60°.

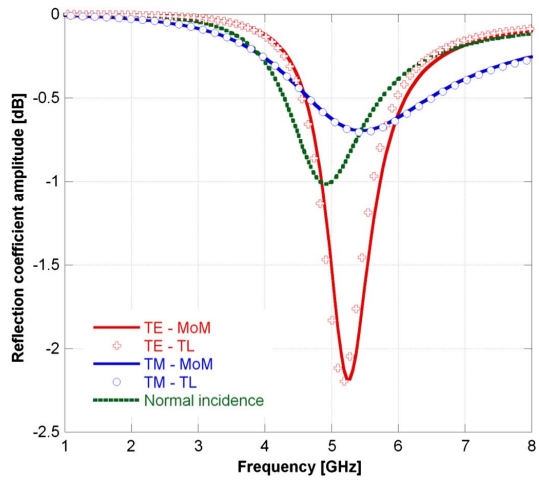

Fig. 15. Reflection coefficient magnitude of the HIS at oblique incidence for TE and TM polarization. Square patch with $D = 10$ mm. Substrate: thickness 3 mm; dielectric permittivity: 4.5-j0.088. Incident angle: 60°.

be more evident with a consequent increment of the reflection losses if a substrate with a lower dielectric permittivity were employed.

VII. Conclusions

The reflection losses of reflectarray antennas have been analyzed by resorting to a simple equivalent transmission line circuit. The closed-form expression of the input impedance (real and imaginary part) of the printed structure has been derived as a function of dielectric substrate loss component and FSS capacitance. It is shown that the real part of the input impedance, which determines the amount of losses, includes two dielectric loss phenomena: the first one is accounted by the real part of the grounded substrate input impedance while the second one, which is present when a periodic array employing perfect conductors is accommodated on a lossy dielectric, is modelled though a series resistor within the FSS impedance. The effect of FSS element geometry and substrate thickness on the reflection losses has been analyzed through some practical examples.

It has been demonstrated that the use of a highly capacitive element, keeping the substrate parameters fixed, leads to the minimization of the reflection losses and to the maximization of the operating bandwidth.

Appendix I
Input Impedance of a Grounded Lossy Substrate

The input impedance of the grounded lossy dielectric slab Z_d is given by:

$$Z_d = j\frac{\zeta_0}{\sqrt{\varepsilon_r' + j\varepsilon_r''}}\tan\left(k_0\sqrt{\varepsilon_r' + j\varepsilon_r''}d\right) \tag{A1}$$

where ζ_0 is the characteristic impedance of free space; k_0 is the free space propagation constant and d is the thickness of the dielectric substrate. The two constituent terms of the relation (A1) can be re-written as follows:

$$\frac{\zeta_0}{\sqrt{\varepsilon_r' + j\varepsilon_r''}} = \frac{\zeta_0}{\gamma}\left[\cos(\alpha) - j\sin(\alpha)\right] \tag{A2}$$

$$\begin{aligned}&\tan\left(k_0\sqrt{\varepsilon_r' + j\varepsilon_r''}d\right)\\ &\quad= \tan\left(k_0 d\gamma\left(\cos(\alpha) + j\sin(\alpha)\right)\right)\\ &\quad= \frac{\tan\left(k_0 d\gamma\cos(\alpha)\right) + j\tanh\left(k_0 d\gamma\sin(\alpha)\right)}{1 - j\tan\left(k_0 d\gamma\cos(\alpha)\right)\cdot\tanh\left(k_0 d\gamma\sin(\alpha)\right)}\end{aligned} \tag{A3}$$

where α and γ are two auxiliary variables which read:

$$\alpha = \frac{1}{2}a\tan\left(\frac{\varepsilon_r''}{\varepsilon_r'}\right);\quad \gamma = \sqrt[4]{\left(\varepsilon_r'\right)^2 + \left(\varepsilon_r''\right)^2} \tag{A4}$$

Assuming verified the low or moderate loss condition ($\varepsilon_r' \gg \varepsilon_r''$) the coefficients in (A4) simplify as follows:

$$\alpha \cong \frac{1}{2}\left(\frac{\varepsilon_r''}{\varepsilon_r'}\right) \ll 1;\quad \gamma \simeq \sqrt{\varepsilon_r'} \tag{A5}$$

Since $\alpha \ll 1$, the quantity $cos(\alpha)$ can be replaced by 1. The input impedance of the grounded lossy substrate is therefore well approximated by the following relation:

$$\begin{aligned}Z_d \cong\ & \frac{\tan\left(k_0 d\sqrt{\varepsilon_r'}\right) + j\tanh\left(k_0 d\left(\frac{\varepsilon_r''}{2\sqrt{\varepsilon_r'}}\right)\right)}{1 - j\tan\left(k_0 d\sqrt{\varepsilon_r'}\right)\cdot\tanh\left(k_0 d\left(\frac{\varepsilon_r''}{2\sqrt{\varepsilon_r'}}\right)\right)}\\ &\times\frac{\zeta_0}{\sqrt{\varepsilon_r'}}\left(\frac{1}{2}\left(\frac{\varepsilon_r''}{\varepsilon_r'}\right) + j\right)\end{aligned} \tag{A6}$$

By manipulating the algebraic relation (A6) and by replacing the operators sin, tan and $tanh$ applied to very small arguments with their first order Taylor expansion, the real and the imaginary parts can be attained (see (A7) and (A8) at bottom of page). The relations (A7) and (A8) can be further simplified for obtaining (9) and (10) since, under the initial assumption $\varepsilon_r' \gg \varepsilon_r''$, the following inequalities are valid:

$$\begin{aligned}&\tan^2\left(k_0 d\sqrt{\varepsilon_r'}\right)\tanh^2\left(k_0 d\frac{\varepsilon_r''}{2\sqrt{\varepsilon_r'}}\right) \ll 1;\\ &\tanh\left(k_0 d\frac{\varepsilon_r''}{2\sqrt{\varepsilon_r'}}\right) \ll 1;\\ &\tan\left(k_0 d\sqrt{\varepsilon_r'}\right)\\ &\quad\gg \frac{\varepsilon_r''}{2\varepsilon_r'}\tanh\left(k_0 d\frac{\varepsilon_r''}{2\sqrt{\varepsilon_r'}}\right)\left(1 + \tan^2\left(k_0 d\sqrt{\varepsilon_r'}\right)\right)\end{aligned} \tag{A9}$$

Appendix II
Demonstration: $B \gg R$ and $B \gg A$

As shown in (3), the real part of the FSS impedance is expressed by:

$$R_D \simeq \frac{-2\varepsilon_r''}{\omega C_0\left(\varepsilon_r' + 1\right)^2} \tag{B1}$$

Around the resonance frequency the absolute value of the FSS reactance is comparable with the reactance of substrate impedance:

$$\left|\frac{1}{\left(\omega C_0\frac{(\varepsilon_r'+1)}{2}\right)}\right| \sim |B| \quad at\ resonance \tag{B2}$$

By substituting the relation (B2) in (B1) and using $\varepsilon_r' \gg \varepsilon_r''$ we obtain:

$$\left|\frac{2\varepsilon_r''}{\omega C_0\left(\varepsilon_r' + 1\right)^2}\right| \sim \left|\frac{\varepsilon_r''}{(\varepsilon_r' + 1)}B\right| \ll B \quad at\ resonance \tag{B3}$$

$$\mathrm{Re}\{Z_d\} \cong \frac{-\frac{\zeta_0}{\sqrt{\varepsilon_r'}}\left[\frac{\varepsilon_r''}{2\varepsilon_r'}\tan\left(k_0 d\sqrt{\varepsilon_r'}\right)\left(1 - \tanh^2\left(k_0 d\frac{\varepsilon_r''}{2\sqrt{\varepsilon_r'}}\right)\right) - \tanh\left(k_0 d\frac{\varepsilon_r''}{2\sqrt{\varepsilon_r'}}\right)\left(1 + \tan^2\left(k_0 d\sqrt{\varepsilon_r'}\right)\right)\right]}{\left(1 + \tan^2\left(k_0 d\sqrt{\varepsilon_r'}\right)\tanh^2\left(k_0 d\frac{\varepsilon_r''}{2\sqrt{\varepsilon_r'}}\right)\right)} \tag{A7}$$

$$\mathrm{Im}\{Z_d\} \cong \frac{\frac{\zeta_0}{\sqrt{\varepsilon_r'}}\left[\tan\left(k_0 d\sqrt{\varepsilon_r'}\right)\left(1 - \tanh^2\left(k_0 d\frac{\varepsilon_r''}{2\sqrt{\varepsilon_r'}}\right)\right) + \frac{\varepsilon_r''}{2\varepsilon_r'}\tanh\left(k_0 d\frac{\varepsilon_r''}{2\sqrt{\varepsilon_r'}}\right)\left(1 + \tan^2\left(k_0 d\sqrt{\varepsilon_r'}\right)\right)\right]}{\left(1 + \tan^2\left(k_0 d\sqrt{\varepsilon_r'}\right)\tanh^2\left(k_0 d\frac{\varepsilon_r''}{2\sqrt{\varepsilon_r'}}\right)\right)}. \tag{A8}$$

In order to demonstrate that the imaginary part of Z_d, B, is much larger than its real part, A, it is useful to re-write the A and B terms as follows:

$$A \cong \frac{\zeta_0}{\sqrt{\varepsilon_r'}} \left[\underbrace{\frac{\varepsilon_r''}{2\varepsilon_r'} \tan\left(k_0 d\sqrt{\varepsilon_r'}\right)}_{negative} - \underbrace{\left(k_0 d \frac{\varepsilon_r''}{2\sqrt{\varepsilon_r'}}\right)\left(1+\tan^2\left(k_0 d\sqrt{\varepsilon_r'}\right)\right)}_{positive} \right] \cong \frac{\zeta_0}{\sqrt{\varepsilon_r'}} \left[\tan\left(k_0 d\sqrt{\varepsilon_r'}\right)\right] \quad \text{(B4)}$$

As highlighted in (B4), A contains only a positive term which is much smaller than B since $\varepsilon_r' \gg \varepsilon_r''$.

Appendix III
Demonstration: $R \gg A$ at the Resonance

The real part of the input impedance of the grounded dielectric substrate (referred to as A) is expressed in relation (B4). In the case of relatively thin substrates (which is typically the case of high-impedance surfaces at the first resonance), $d < \lambda_g/8$, the argument of the tan function in (B4) is smaller than $\pi/4$. Under this assumption, the tan operator can be replaced with its first order Taylor expansion leading to:

$$A \approx -\frac{\zeta_0}{\sqrt{\varepsilon_r'}} \left(k_0^3 d^3 \frac{\varepsilon_r''\sqrt{\varepsilon_r'}}{2}\right) \quad \text{(C1)}$$

The expression of the real part of the FSS impedance can be found in (B1). At the resonance, as shown in (17), the absolute value of the reactance of the substrate impedance is almost equal to the absolute value of the reactance of the FSS impedance. By substituting (17) in (B1) and by replacing the tangent operator with its first order Taylor expansion we obtain:

$$R_D \simeq \frac{\zeta_0}{\sqrt{\varepsilon_r'}} \frac{-\varepsilon_r''}{(\varepsilon_r'+1)} \left(k_0 d\sqrt{\varepsilon_r'}\right) \quad \text{(C2)}$$

Hence, R_D is larger than A if the following inequality holds:

$$\underbrace{k_0^2 d^2 \varepsilon_r'}_{<\left(\frac{\pi}{4}\right)^2} + \underbrace{k_0^2 d^2}_{\ll\left(\frac{\pi}{4}\right)^2} \ll 2 \quad \text{(C3)}$$

The first term is the square value of the tangent argument. Since the argument of the tangent has been initially supposed lower than $\pi/4$, the first term is much smaller than $(\pi/4)^2$ and, consequently, so is the second term.

References

[1] D. M. Pozar, S. D. Targonski, and H. D. Syrigos, "Design of millimeter wave microstrip reflectarrays," *IEEE Trans. Antennas Propag.*, vol. 45, pp. 287–296, Feb. 1997.

[2] J. A. Encinar, "Design of two-layer printed reflectarrays using patches of variable size," *IEEE Trans. Antennas Propag.*, vol. 49, pp. 1403–1410, Oct. 2001.

[3] D. M. Pozar, S. D. Targonski, and R. Pokuls, "A shaped-beam microstrip patch reflectarray," *IEEE Trans. Antennas Propag.*, vol. 47, no. 7, pp. 1167–1173, Jul. 1999.

[4] M. Arrebola, J. A. Encinar, and M. Barba, "Multi-fed printed reflectarray with three simultaneous shaped beams for LMDS central station antenna," *IEEE Trans. Antennas Propag.*, vol. 56, no. 6, pp. 1518–1527, Jun. 2008.

[5] D. Sievenpiper, L. Zhang, R. F. J. Broas, N. G. Alexopolous, and E. Yablonovitch, "High-impedance electromagnetic surfaces with a forbidden frequency band," *IEEE Trans. Microw. Theory Tech.*, vol. 47, no. 11, pp. 2059–2074, 1999.

[6] F. Costa, A. Monorchio, and G. Manara, "Analysis and design of ultra thin electromagnetic absorbers comprising resistively loaded high impedance surfaces," *IEEE Trans. Antennas Propag.*, vol. 58, no. 5, 2010.

[7] F. Costa, O. Luukkonen, C. R. Simovski, A. Monorchio, S. A. Tretyakov, and P. De Maagt, "TE surface wave resonances on high-impedance surface based antennas: Analysis and modeling," *IEEE Trans. Antennas Propag.*, vol. 59, no. 10, pp. 3588–3596, 2011.

[8] R. Kelly, T. Kokkinos, and A. P. Feresidis, "Analysis and design of sub-wavelength resonant cavity type 2-D leaky-wave antennas," *IEEE Trans. Antennas Propag.*, vol. 56, no. 9, pp. 2817–2825, 2008.

[9] R. Abhari and G. V. Eleftheriades, "Metallo-dielectric electromagnetic bandgap structures for suppression and isolation of the parallel-plate noise in high-speed circuits," *IEEE Trans. Microw. Theory Tech.*, vol. 51, no. 6, pp. 1629–1639, Jun. 2003.

[10] A. P. Feresidis, G. Goussetis, A. Yakovlev, and C. Simovski, "High impedance surfaces: Applications," in *Metamaterial Handbook*. London, U.K.: Taylor and Francis, vol. II, ch. 22.

[11] D. F. Sievenpiper, J. H. Schaffner, H. J. Song, R. Y. Loo, and G. Tangonan, "Two-dimensional beam steering using an electrically tunable impedance surface," *IEEE Trans. Antennas Propag.*, vol. 51, no. 10, pp. 2713–2722, 2003.

[12] D. M. Pozar, "Wideband reflectarrays using artificial impedance surfaces," *Electron. Lett.*, vol. 43, no. 3, pp. 148–149, Feb. 2007.

[13] F. Costa, S. Genovesi, and A. Monorchio, "On the bandwidth of high-impedance frequency selective surfaces," *IEEE Antennas Wireless Propag. Lett.*, vol. 8, pp. 1341–1344, 2009.

[14] M. Bozzi, S. Germani, and L. Perregrini, "Performance comparison of different element shapes used in printed reflectarrays," *Antennas Wireless Propag. Lett.*, vol. 2, no. 1, pp. 219–222, 2003.

[15] M. Bozzi, S. Germani, and L. Perregrini, "A figure of merit for losses in printed reflectarray elements," *Antennas Wireless Propag. Lett.*, vol. 3, no. 1, pp. 257–260, 2004.

[16] H. Rajagopalan and Y. Rahmat-Samii, "On the reflection characteristics of a reflectarray element with low-loss and high-loss substrates," *IEEE Antennas Propag. Mag.*, vol. 52, no. 4, pp. 73–89, Aug. 2010.

[17] M. I. Abbasi and M. Y. Ismail, "Reflection loss and bandwidth performance of X-band infinite reflectarrays: Simulations and measurements," *Microw. Opt. Technol. Lett.*, vol. 53, no. 1, pp. 77–80, 2011.

[18] F. Costa, A. Monorchio, and G. Manara, "Efficient analysis of frequency selective surfaces by a simple equivalent circuit approach," *IEEE Antennas Propag. Mag.*, to be published.

[19] F. Costa, A. Monorchio, and G. Manara, "An equivalent-circuit modeling of high impedance surfaces employing arbitrarily shaped FSS," in *Proc. Int. Conf. on Electromagnetics in Advanced Applications, ICEEA*, Turin, Sep. 14–18, 2009, pp. 852–855.

[20] O. Luukkonen, C. Simovski, G. Granet, G. Goussetis, D. Lioubtchenko, A. V. Räisänen, and S. A. Tretyakov, "Simple and accurate analytical model of planar grids and high-impedance surfaces comprising metal strips or patches," *IEEE Trans. Antennas Propag.*, vol. 56, no. 6, pp. 1624–1632, 2008.

[21] G. L. Johnson, Solid State Tesla Coil Ch.3- Lossy Capacitors, Dec. 10, 2001.

[22] S. A. Tretyakov and C. R. Simovski, "Dynamic model of artificial reactive impedance surfaces," *J. Electromagn. Waves Appl.*, vol. 17, no. 1, pp. 131–145, 2003.

[23] R. Mittra, C. Chan, and T. Cwik, "Techniques for analyzing frequency selective surfaces: A review," *IEEE Proc.*, vol. 76, pp. 1593–1615, Dec. 1988.

[24] J. Ethier, M. R. Chaharmir, and J. Shaker, "Novel approach for low-loss reflectarray designs," in *Proc. IEEE Int. Symp. on Antennas Propag.*, Jul. 3–8, 2011, pp. 373–376.

[25] P. Nayeri, F. Yang, and A. Z. Elsherbeni, "Bandwidth improvement of reflectarray antennas using closely spaced elements," *Progr. Electromagn. Res. C*, vol. 18, pp. 19–29, 2011.
[26] D. Pozar and S. Targonski, "A microstrip reflectarray using crossed dipoles," in *Proc. IEEE Int. Symp. on Antennas Propag.*, Jun. 1998, vol. 2, pp. 1008–1011.
[27] E. Irci, K. Sertel, and J. L. Volakis, "An extremely low profile, compact, and broadband tightly coupled patch array," *Radio Sci.*, vol. 47, 2012.
[28] C. L. Holloway and E. F. Kuester, "Net and partial inductance of a microstrip ground plane," *IEEE Trans. Electromagn. Compat.*, vol. 40, no. 2, pp. 33–46, 1998.

Filippo Costa (S'07–M'10) was born in Pisa, Italy, on October 31, 1980. He received the M.Sc. degree in telecommunication engineering and the Ph.D. degree in applied electromagnetism in electrical and biomedical engineering, electronics, smart sensors, nano-technologies from the University of Pisa, Pisa, Italy, in 2006 and 2010, respectively.

From March to August 2009, he was a Visiting Researcher at the Department of Radio Science and Engineering, Helsinki University of Technology, TKK (now Aalto University), Finland. From January 2010 he is a Postdoctoral Researcher at the University of Pisa. His research is focused on the analysis and modelling of Frequency Selective Surfaces and Artificial Impedance Surfaces with emphasis to their application in electromagnetic absorbing materials, antennas, radomes, waveguide filters and techniques for retrieving dielectric permittivity of materials.

Agostino Monorchio (S'89–M'96–SM'04–F'12) received the Laurea degree in electronics engineering and the Ph.D. degree in methods and technologies for environmental monitoring from the University of Pisa, Pisa, Italy, in 1991 and 1994, respectively.

During 1995, he joined the Radio Astronomy Group, Arcetri Astrophysical Observatory, Florence, Italy, as a Postdoctoral Research Fellow, in the area of antennas and microwave systems. He has been collaborating with the Electromagnetic Communication Laboratory, Pennsylvania State University (Penn State), University Park, and he is an Affiliate of the Computational Electromagnetics and Antennas Research Laboratory. He has been a Visiting Scientist at the University of Granada, Spain, and at the Communication University of China in Beijing. He is currently an Associate Professor in the School of Engineering, University of Pisa, and Adjunct Professor at the Italian Naval Academy of Livorno. He is also an Adjunct Professor in the Department of Electrical Engineering, Penn State. He is on the Teaching Board of the Ph.D. course in "Remote Sensing" and on the council of the Ph.D. School of Engineering "Leonardo da Vinci" at the University of Pisa. His research interests include the development of novel numerical and asymptotic methods in applied electromagnetics, both in frequency and time domains, with applications to the design of antennas, microwave systems and RCS calculation, the analysis and design of frequency-selective surfaces and novel materials, and the definition of electromagnetic scattering models from complex objects and random surfaces for remote sensing applications. He has been a reviewer for many scientific journals and he has been supervising various research projects related to applied electromagnetic, commissioned and supported by national companies and public institutions.

Dr. Monorchio has served as Associate Editor of the IEEE ANTENNAS AND WIRELESS PROPAGATION LETTERS. He received a Summa Foundation Fellowship and a NATO Senior Fellowship.